Nuclear Instruments and Methods in Physics Research A 767 (2014) 34–40

Contents lists available at ScienceDirect

Nuclear Instruments and Methods in Physics Research A

journal homepage: www.elsevier.com/locate/nima

# Performance of the reconstruction algorithms of the FIRST experiment pixel sensors vertex detector

R. Rescigno [r,*], Ch. Finck [r], D. Juliani [r], E. Spiriti [e,g], J. Baudot [r], Z. Abou-Haidar [p], C. Agodi [f], M.A.G. Alvarez [p], T. Aumann [a], G. Battistoni [b], A. Bocci [p], T.T. Böhlen [v,w], A. Boudard [u], A. Brunetti [c,m], M. Carpinelli [c,m], G.A.P. Cirrone [f], M.A. Cortes-Giraldo [q], G. Cuttone [f], M. De Napoli [f], M. Durante [a], M.I. Gallardo [q], B. Golosio [c,m], E. Iarocci [e,j], F. Iazzi [h,k], G. Ickert [a], R. Introzzi [h], J. Krimmer [t], N. Kurz [a], M. Labalme [s], Y. Leifels [a], A. Le Fevre [a], S. Leray [u], F. Marchetto [h], V. Monaco [h,l], M.C. Morone [i,n], P. Oliva [c,m], A. Paoloni [e], V. Patera [g,j], L. Piersanti [e,j], R. Pleskac [a], J.M. Quesada [q], N. Randazzo [f], F. Romano [f,o], D. Rossi [a], M. Rousseau [r], R. Sacchi [h,l], P. Sala [b], A. Sarti [e,j], C. Scheidenberger [a], C. Schuy [a], A. Sciubba [g,j], C. Sfienti [f,w], H. Simon [a], V. Sipala [c], S. Tropea [f], M. Vanstalle [r], H. Younis [h,k,d,x]

[a] GSI Helmholtzzentrum für Schwerionenforschung, Darmstadt, Germany
[b] Istituto Nazionale di Fisica Nucleare - Sezione di Milano, Italy
[c] Istituto Nazionale di Fisica Nucleare - Sezione di Cagliari, Italy
[d] Istituto Nazionale di Fisica Nucleare - Sezione di Catania, Italy
[e] Istituto Nazionale di Fisica Nucleare - Laboratori Nazionali di Frascati, Italy
[f] Istituto Nazionale di Fisica Nucleare - Laboratori Nazionali del Sud, Italy
[g] Istituto Nazionale di Fisica Nucleare - Sezione di Roma 3, Italy
[h] Istituto Nazionale di Fisica Nucleare - Sezione di Torino, Italy
[i] Istituto Nazionale di Fisica Nucleare - Sezione di Roma Tor Vergata, Italy
[j] Dipartimento di Scienze di Base e Applicate per l'Ingegneria, "La Sapienza" Università di Roma, Italy
[k] Dipartimento di Fisica, Politecnico di Torino, Italy
[l] Dipartimento di Fisica, Università di Torino, Italy
[m] Università di Sassari, Italy
[n] Dipartimento di Biopatologia e Diagnostica per Immagini, Università di Roma Tor Vergata, Italy
[o] Centro Studi e Ricerche e Museo Storico della Fisica "Enrico Fermi", Roma, Italy
[p] CNA, Sevilla, Spain
[q] Departamento de Fisica Atomica, Molecular y Nuclear, University of Sevilla, 41080-Sevilla, Spain
[r] Institut Pluridisciplinaire Hubert Curien, 23 rue du Loess, 67037 Strasbourg Cedex 2, France
[s] LPC-Caen, ENSICAEN, Université de Caen, CNRS/IN2P3, Caen, France
[t] IPN-Lyon, Université de Lyon, Université Lyon 1, CNRS/IN2P3, Villeurbanne, France
[u] CEA-Saclay, IRFU/SPhN, Gif sur Yvette Cedex, France
[v] European Organization for Nuclear Research CERN, Geneva, Switzerland
[w] Medical Radiation Physics, Karolinska Institutet and Stockholm University, Stockholm, Sweden
[x] Université Mainz Johann-Joachim-Becher, Mainz, Germany

ARTICLE INFO

*Article history:*
Received 10 January 2014
Received in revised form
22 July 2014
Accepted 19 August 2014
Available online 24 August 2014

ABSTRACT

Hadrontherapy treatments use charged particles (e.g. protons and carbon ions) to treat tumors. During a therapeutic treatment with carbon ions, the beam undergoes nuclear fragmentation processes giving rise to significant yields of secondary charged particles. An accurate prediction of these production rates is necessary to estimate precisely the dose deposited into the tumours and the surrounding healthy tissues. Nowadays, a limited set of double differential carbon fragmentation cross-section is available.

* Corresponding author. Tel.: +33388106176; fax: +33388106292.
*E-mail address:* regina.rescigno@iphc.cnrs.fr (R. Rescigno).

http://dx.doi.org/10.1016/j.nima.2014.08.024

*Keywords:*
CMOS active pixel sensors
Vertex detector
Clustering
Tracking
Vertexing

Experimental data are necessary to benchmark Monte Carlo simulations for their use in hadrontherapy. The purpose of the FIRST experiment is to study nuclear fragmentation processes of ions with kinetic energy in the range from 100 to 1000 MeV/u. Tracks are reconstructed using information from a pixel silicon detector based on the CMOS technology. The performances achieved using this device for hadrontherapy purpose are discussed. For each reconstruction step (clustering, tracking and vertexing), different methods are implemented. The algorithm performances and the accuracy on reconstructed observables are evaluated on the basis of simulated and experimental data.


## 1. Introduction

The use of charged hadrons in cancer therapy was first considered by Wilson [1] and is motivated by the highly localised dose distribution that these particles provide at the end of their range *i.e.* the Bragg peak. Charged particles heavier than protons (*i.e.* $^{12}C$) have additional advantages like the reduced lateral scattering and the increased relative biological effectiveness (RBE) at the end of their range, making them well-suited for the treatment of tumours resistant to photon radiation. However, as carbon nuclei penetrate the human tissues, they undergo inelastic nuclear reactions leading to the production of secondary fragments lighter than primary ions. Such fragments have different ranges and angular distributions with respect to carbons and they contribute to the dose distribution inside and outside the tumour [2]. Therefore accurate fragmentation studies are needed to estimate the biological dose [3].

Treatment planning system is currently based on deterministic codes [4,5] which are relatively fast. Nevertheless, analytical calculations are often benchmarked against Monte-Carlo simulations in order to test and improve their accuracy [6,7]. In the past, several measurements of fragment yields and total cross-section were made [8–10]. The comparison between nuclear reaction model predictions and experimental data has shown a discrepancy up to an order of magnitude for double-differential quantities (DDCS) with respect to kinetic energy and scattering polar angle [7,11,12]. These results suggest the need to improve the Monte-Carlo simulation for their application in hadrontherapy. However, a limited set of experimental data is available in the literature. In this framework, the FIRST (Fragmentation of Ions Relevant for Space and Therapy) experiment aims to measure DDCS for light ions in the kinetic energy range between 100 and 1000 MeV/u [13–17].

The trajectory of the charged particles emerging from the target is measured by the *Vertex detector*. This device is composed of four planes of MIMOSA26 (M26) [18] sensors, separated by 2 mm, with a distance of 6 mm between the first plane and the target center. The M26 sensor has a sensitive area of 10.6 mm × 20.2 mm and the active part consists of 576 lines and 1152 columns of pixels with a pitch of 18.4 μm. The output is binary: the pixel is considered fired when the charge deposited is higher than a given threshold. The spatial resolution of such device for minimum ionizing particles (MIP) is better than 4 μm [18].

Originally designed to detect the MIPs, M26 sensor is used, in FIRST experiment, to track high ionizing particles. In this work we discuss the performances achieved using this device for hadrontherapy purpose. A set of dedicated reconstruction methods is developed in order to retrieve the particle impact positions on each sensor, the particle trajectories and the fragmentation points. The aim of this paper is to evaluate the performances of these algorithms and the accuracy achieved on the reconstructed observables.

Reconstruction algorithms for clustering, tracking and vertexing are presented in the next section. In Section 3 algorithm performances are evaluated and a comparison between simulated and experimental data is made.

## 2. Reconstruction software

The reconstruction algorithms for the *Vertex detector* are implemented in the framework of FIRST software [19] and based on Root libraries [20]. The code is organized in modules corresponding to each reconstruction step to maximize the flexibility in using the different algorithms.

The vertex sub-package can read back raw data files as well as the output of the simulation. The reconstruction software chain is organized in three steps: first, the fired pixels are gathered to identify clusters on each plane (*clustering*); aligned clusters on different planes are searched to build a track (*tracking*) and, finally, reconstructed tracks are used to estimate the vertex position (*vertexing*). For each reconstruction step at least two algorithms were implemented.

### 2.1. Clustering

The energy deposited by an ionizing particle impinging a M26 sensor produces charge carriers that are collected by a number of adjacent pixels. The clustering procedure aims to find out fired pixels (hits) originated by a single particle. Each pixel is identified by a line and a column number.

Two *clustering* algorithms were implemented using two different approaches, both based on the *first neighbour* search. Two pixels are called *first neighbours* if they are contiguous in line or column *i.e.* if their line (column) number is the same and the difference between their column (line) number is equal to one. For both algorithms, fired pixels are organised in a list.

The first algorithm performs the *first neighbour* search in an iterative way. To build a cluster a pixel of the list is selected. A procedure checks if its first neighbours are fired and if it happens these pixels are added to the current cluster. Subsequently, each of them is used as a starting point for the next *first neighbour* search. The procedure for a single cluster stops when no more first neighbours are found. Pixels from the list not belonging to any cluster are used as starting point to build a new cluster.

In the second method, fired pixels are sorted first by lines and then by columns. Each line is scanned, and the *first neighbour* search is performed for each fired pixel.

### 2.2. Tracking

To reconstruct a track, information about the cluster positions on each sensor is needed. A sequence of at least three aligned clusters (three out of four planes of the *Vertex detector*) is required to build a track. Three different methods were implemented: two of them are called *local* procedures and the last one is based on the Hough transform [21].

#### 2.2.1. Local method with BM (TrackingBM)

*TrackingBM* needs the position of the impinging particle at the target level to start the track reconstruction. This information is provided by the Beam Monitoring (BM) of the FIRST experiment. Located upstream the target, the BM is a drift chamber filled by an

$Ar–CO_2$ 80–20% gas mixture. This detector provides the beam trajectory and the ion impinging point on the target with a spatial resolution of about 140 μm [16].

The beam track reconstructed in the BM is projected to the center of the target. A *road* is defined by a straight line connecting the projected point and the cluster of the last plane (farthest from the target). The intersection of the *road* with the next plane is computed and the algorithm looks for a cluster close to the projected road within a given tolerance (adjustable parameter depending on the azimuthal angle of the track). In this case, the cluster is added to the track and the track parameters (slopes and offsets) are computed by fitting the cluster coordinates (*i.e.* center of gravity of the pixels) with a 3D line in space. If no cluster is found the track is extrapolated to the next plane. The single track reconstruction stops when the more upstream plane is reached. Subsequently, a new cluster of the last plane is considered to build a new track.

The whole procedure stops when no cluster on the last plane is left.

#### 2.2.2. Local method (TrackingL)

This method is based on a combinatorial procedure. The algorithm starts searching for all possible combinations between the clusters of the last plane and the previous plane building the so-called *micro-tracks*. In the next step, each of these *micro-tracks* is extrapolated to the following plane, looking for clusters that may be a good candidate to belong to the track. From this point on, the algorithm works in the same way as described before.

At the energies used in FIRST experiment, clusters from protons are composed, on average, by 4 pixels. Heavier particles usually produce larger clusters [22]. A noisy cluster is usually a single pixel. Since a combinatorial procedure is applied, the use of noisy cluster to build a track is more likely. In order to minimize the number of fake tracks (*i.e.* tracks built using noisy clusters), only clusters having more than one pixel are considered.

#### 2.2.3. Hough transform (TrackingH)

The classical 2D Hough transform can be used for tracking because of its straight lines detection abilities. A straight line parameterized as $y = mx + b$ in a Cartesian space $(X,Y)$ corresponds to a point in the Hough parameter space $(m, b)$ while a point in the Cartesian space is associated to a straight line in the Hough space. Then a sequence of aligned clusters in a Cartesian space appears in the Hough space as a set of lines having a common intersection point. The tracking is performed in the Hough parameter space, searching for all intersection points. Each point is found minimizing the distance between tracks, using parameters tuned for the FIRST geometry. To save computing time, the 2D Hough transform is applied independently in the $(X,Z)$ projection and in $(Y,Z)$ projection, $Z$ being the beam axis.

### 2.3. Vertexing

The vertex is defined as the common position from where two or more tracks are generated. To locate this point, two different algorithms were implemented, both based on a minimization criterion: in the first procedure a variable that quantifies the distance between tracks is minimized (*Impact Parameter Approach*); in the second one the probability to find two or more tracks in the same point is maximized (*Probability Distribution Approach*).

#### 2.3.1. Impact parameter approach

This method aims to identify the point where the closest approach of tracks to the vertex occurs. The vertex location is identified by three coordinates. To find the vertex coordinate longitudinal to the beam ($Z$ direction), planes of the target volume orthogonal to the beam axis are considered. Each track is extrapolated on a given plane and the gravity center of the tracks (centroid of transversal track positions) on this plane is evaluated. The distance between each track and this point is computed. The average of such distances is minimized as a function of the $z$ value. The minimization process is based on a binary search algorithm [23] to improve the convergence time respect to a linear search algorithm [24] and to avoid problems deriving to the step choice. The $Z$ coordinate that minimize the mean distance is the $Z$ vertex position. The gravity center of all tracks computed at this $z$ value is taken as vertex transversal positions.

#### 2.3.2. Probability distribution approach

This vertexing algorithm is based on the topological vertex reconstruction method proposed in Ref. [25]. In this section a review of this method is presented. The search is based on a minimization function $Q(\boldsymbol{v})$ which quantifies the probability to find a vertex at position $\boldsymbol{v}$. A Gaussian probability density tube is constructed around each track, the width of the tube is given by the dispersion of the track:

$$f_i(\boldsymbol{v}) = \exp\left[-\tfrac{1}{2}(\boldsymbol{v}-\boldsymbol{r}_i)^T \boldsymbol{V}_i^{-1}(\boldsymbol{v}-\boldsymbol{r}_i)\right]$$

where $\boldsymbol{r}_i$ is the point of closest distance approach of track $i$ to point $\boldsymbol{v}$, and the $\boldsymbol{V}_i$ is the covariance matrix of the track at $\boldsymbol{r}_i$. In our case, the covariance matrix contains errors on track position. The diagonal elements represent the position uncertainty on $X$, $Y$ or $Z$ direction due to detector spatial resolution, whereas off-diagonal elements represent the correlation between the errors in two different directions. Since measurements in each direction are all independent of each other, the covariance matrix is diagonal.

The vertex function $Q(\boldsymbol{v})$ is defined as

$$Q(\boldsymbol{v}) = \sum_{i=0}^{n} f_i(\boldsymbol{v}) - \frac{\sum_{i=0}^{n} f_i^2(\boldsymbol{v})}{\sum_{i=0}^{n} f_i(\boldsymbol{v})}$$

The value $\hat{\boldsymbol{v}}$ that maximizes the function $Q(\boldsymbol{v})$ corresponds to the most probable vertex position. The existence of a maximum is ensured by the mathematical form of the $Q(\boldsymbol{v})$ function: $Q(\boldsymbol{v}) \simeq 0$ if $f_i(\boldsymbol{v})$ is significant (*i.e.* $f_i(\boldsymbol{v}) \not\simeq 0$) for less than two tracks [25].

A first estimation of $\hat{\boldsymbol{v}}$ is performed using all tracks. In a second step, tracks not compatible with the vertex (*i.e* for which $f_i(\hat{\boldsymbol{v}})$ value is less than a given threshold) are discarded and used for a new vertex candidate.

## 3. Evaluation of the algorithm performances

The performances of the clustering, tracking and vertexing algorithms were evaluated using 50,000 carbon ions simulated events with the GEANT4 [26] package (version 4.9.5.1). The *Vertex detector* characteristics and the experimental conditions of the FIRST experiment (target thickness, kinetic energy of the beam) were modeled. The detector response for charged particles was simulated in order to reproduce the cluster features. This response depends on the energy deposited in the active part of the sensor. A set of FIRST experimental data [22] was used to implement a phenomenological model. Dedicated runs without target were used. Since the experimental sample does not give access to the deposited energy, the model was built as a function of the particle type and of the initial energy of the beam. For this reason, the experimental runs used to characterize the detector were performed with a given specie of particles (protons and carbon ions) at a given energy (80 MeV/u and 400 MeV/u) and at a given beam position.

The distribution of the number of pixel per cluster obtained for a sample of 400 MeV/u carbon ions is reported in Fig. 1 for the

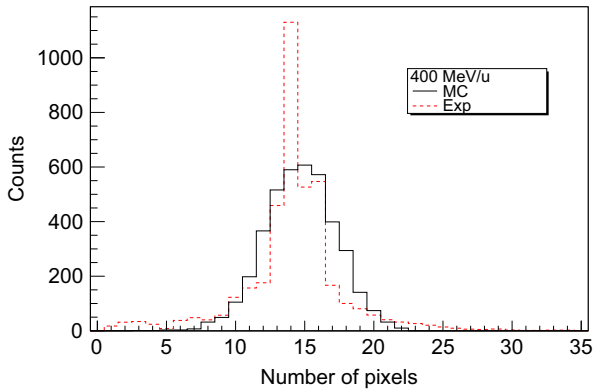


**Fig. 1.** Cluster size distributions for a sample of carbon ions at 400 MeV/u for simulated (solid line) and experimental data (dashed line).

experimental (dashed line) and simulated (solid line) samples. The experimental distribution presents a peak for a number of pixels equal to 14. This is due to the binary response of the pixel that, for a given particle energy and position, leads to a favoured configuration in the distribution. This distribution has a mean value of 14.2 that is in good agreement with the one obtained with our model (14.6). The standard deviation is slightly higher for simulated data (about 10%). The impact of these differences on track resolution was estimated to be less than 5%.

The FIRST BM was not simulated therefore the position of the beam is assumed to be exactly known. In this section, the algorithm efficiency as well as a comparison with data taken during FIRST campaign are presented. The experiment was performed using 400 MeV/u $^{12}$C impinging on a 8 mm thick graphite target.

### 3.1. Clustering

The performances of the clustering algorithms described previously (Section 2.1) are presented in this section. The clustering efficiency was evaluated, for both algorithms, by using a random cluster generator. This device was able to provide a high number of regular and irregular cluster geometrical shapes. The ability of the algorithms to reconstruct the correct shape and size was investigated. The presence of noisy pixels was also taken into account on the base of experimental data.

Both algorithms were able to recognize and reconstruct all clusters (efficiency greater than 99.9%). However, the algorithm based on the iterative procedure is used in the analysis of FIRST data, being 10% faster than the second one.

### 3.2. Tracking

To compare the three tracking methods, the tracks reconstruction efficiency (computed as a ratio of reconstructed and reconstructible tracks) and the proportion of fake reconstructed tracks were evaluated. Reconstructible tracks are the ones generated by particles emitted within the acceptance of the *Vertex detector*. In the simulation, a well reconstructed track has at least three clusters associated to the same particle otherwise it is considered as fake. Furthermore, noisy pixels are randomly generated, according to experimental data. Results on track reconstruction efficiency and on the fraction of fake tracks are reported in Table 1. The three algorithm efficiencies are comparable but the proportion of fake tracks is slightly different. The enhancement of fake tracks arises from the different approaches used to build the tracks. The local method (*TrackingL*) and the Hough transform (*TrackingH*) are based on a combinatorial procedure. The better result is obtained

**Table 1**
Efficiency and fake tracks proportion computed for the three tracking reconstruction algorithms (simulated data).

| | *TrackingBM* | *TrackingL* | *TrackingH* |
|---|---|---|---|
| Efficiency | $(98.7 \pm 0.1)\%$ | $(98.9 \pm 0.1)\%$ | $(99.0 \pm 0.1)\%$ |
| Fake tracks | $(1.99 \pm 0.01)\%$ | $(2.19 \pm 0.01)\%$ | $(2.86 \pm 0.01)\%$ |

**Table 2**
Tracking efficiencies and associated errors for different charge values of detected particles (simulated data).

| Z | 1 | 2 | 3 | 4 | 5 | 6 |
|---|---|---|---|---|---|---|
| Efficiency (%) | 93.6 | 88.9 | 97.5 | 97.7 | 98.8 | 99.9 |
| Error (%) | 0.3 | 0.6 | 0.7 | 0.8 | 0.4 | 0.1 |

using the local method *TrackingBM* in which the beam position information allows minimizing the number of fake tracks. This latter method will be used in the following sections.

Table 2 reports the tracks reconstruction efficiency for different particle charges ($Z=1$ to 6). The efficiency is greater than 90% for all species of particles apart from particles with $Z=2$. Indeed, alpha particles are produced in pair or triplet with a small angle and they exhibit a tendency to move in the same direction. This means that clusters produced by these particles are very close and a mismatch in the track identification can occur.

The coordinates of the particle impact point ($X_{rec}$ and $Y_{rec}$) onto the sensor were calculated by using information from a reconstructed track. These values were compared with the corresponding Monte-Carlo position ($X_{true}$ and $Y_{true}$). In order to evaluate the intrinsic resolution of the reconstruction algorithm the difference between these two quantities was computed. The results are shown in Fig. 2. A Gaussian fit, limited to a range defined by 4 times the RMS of the distribution, was performed. The resolutions, evaluated by such fit, are better than $\sigma = 3$ μm in $X$ and $Y$ directions. An interval is defined with size given by 4 times the fitted sigma. The number of events outside this range (tails) was found to be less than 4% compared with an expectation of 0.006% for the case of a perfect Gaussian.

The distribution of residuals, defined as the distance between the cluster centroid position and the position of the intercept of the reconstructed track in the different planes, is shown in Fig. 3 for simulated events and experimental data. On the left, the contribution of beam tracks (straight lines) is shown: the resolution, for both samples, is better than 6 μm and a proportion of tail consistent with zero for simulation and less than 9% for experimental data is found. The distributions for fragmented particle tracks (more tilted) show more important tails (proportion of 9% for simulated compared with 15% for experimental data) and, for both samples, a resolution less than 10 μm. A difference between experimental and simulated data in the tail distribution can be observed. It could be related to the polar angular rotation of the beam axis with respect to the symmetry axis of *Vertex detector* ($\theta \sim 1^\circ$). This rotation was not taken into account in the simulation.

In conclusion, the different tracking algorithms have an efficiency higher than 98% with a proportion of fake tracks lower than 3%. The resolution is better than 10 μm for fragmented events and it is well reproduced with MC simulation. The proportion of events in the tail stays below 15% in any case, although there is a difference between experimental and simulated data.

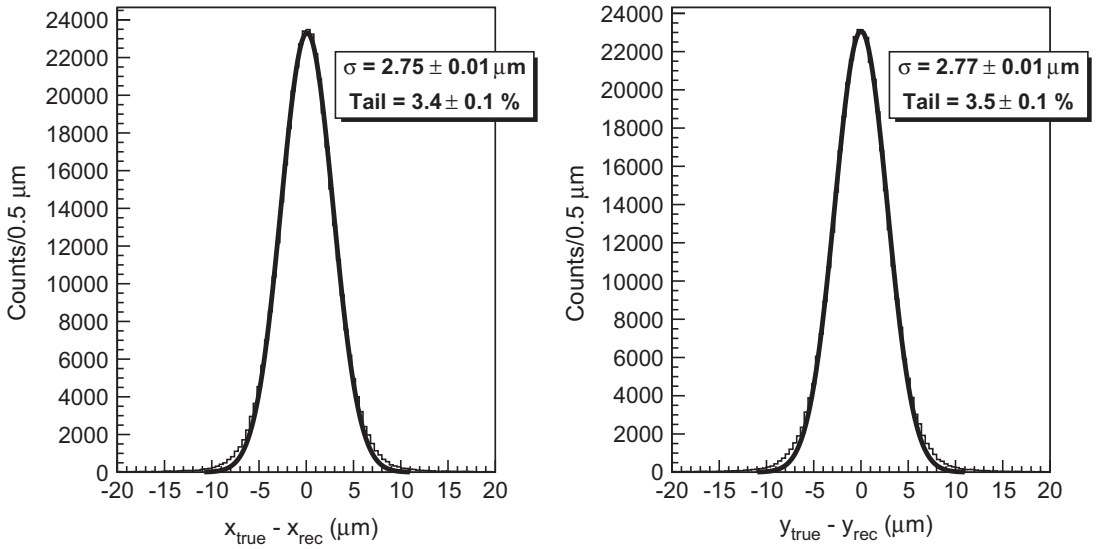


**Fig. 2.** Difference between Monte-Carlo (*true*) and reconstructed (*rec*) position in *X* and *Y* direction. The result of a Gaussian fit is shown with the associated proportion events outside $\pm 4\sigma$ (tails).

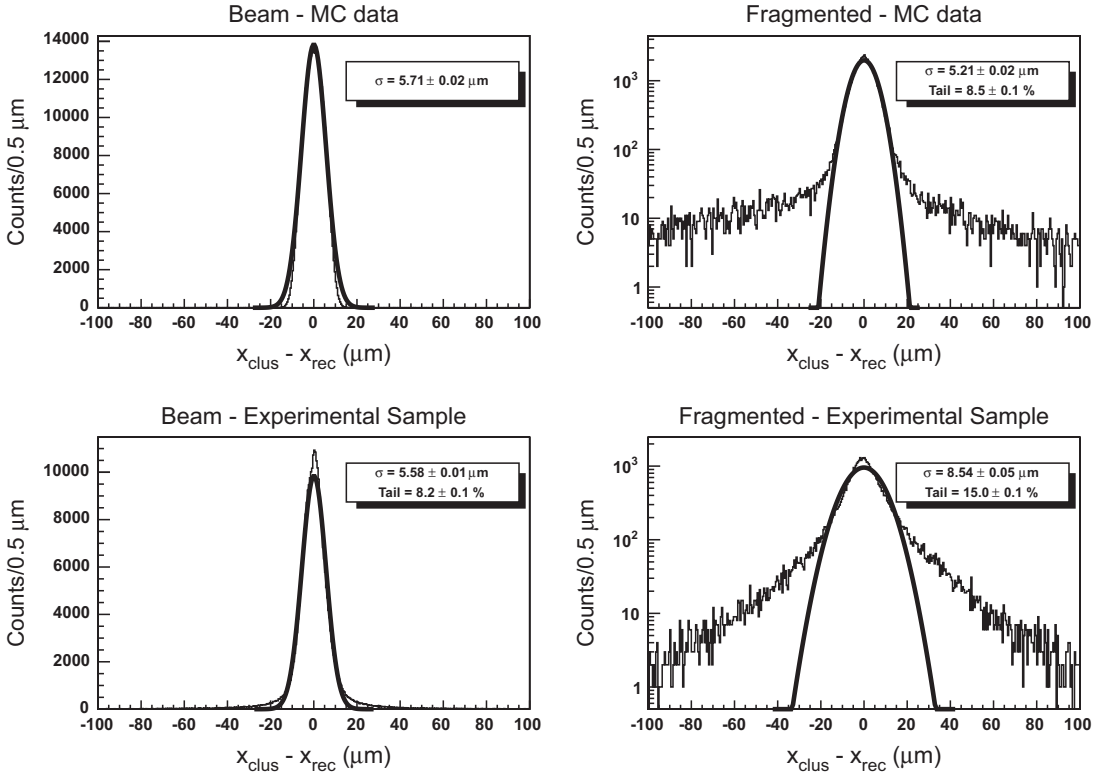


**Fig. 3.** Residual distance between the cluster position and the reconstructed track position for impinging carbon beam events (left) and fragmented events (right). Results are shown for Monte-Carlo (top) and for experimental data (bottom).

### 3.3. Vertexing

The performances of the two vertex reconstruction methods were compared. The efficiency and the proportion of fake vertices are reported in Table 3: for both algorithms an efficiency close to 99% is reached with a proportion of fake vertices of ~3%. However, in both cases, the 3/4 of the about 1% inefficiency arises from tracking, typically in a fragmented event in which two tracks are produced but only one is reconstructed. The number of fake vertices is totally affected by tracking limitation: all fake vertices arise from non-fragmented events in which a fake track is reconstructed.

**Table 3**
Efficiency and proportion of fake vertices computed with the two vertex reconstruction algorithms.

| | Impact parameter approach | Probability approach |
|---|---|---|
| Efficiency | (98.7 ± 0.2)% | (98.6 ± 0.2)% |
| Fake vertices | (2.30 ± 0.01)% | (2.30 ± 0.01)% |

The difference between Monte-Carlo generated (*true*) and reconstructed (*rec*) vertex positions is shown in Fig. 4 for *X* (left) and *Y* (right) directions and in Fig. 5 for the longitudinal

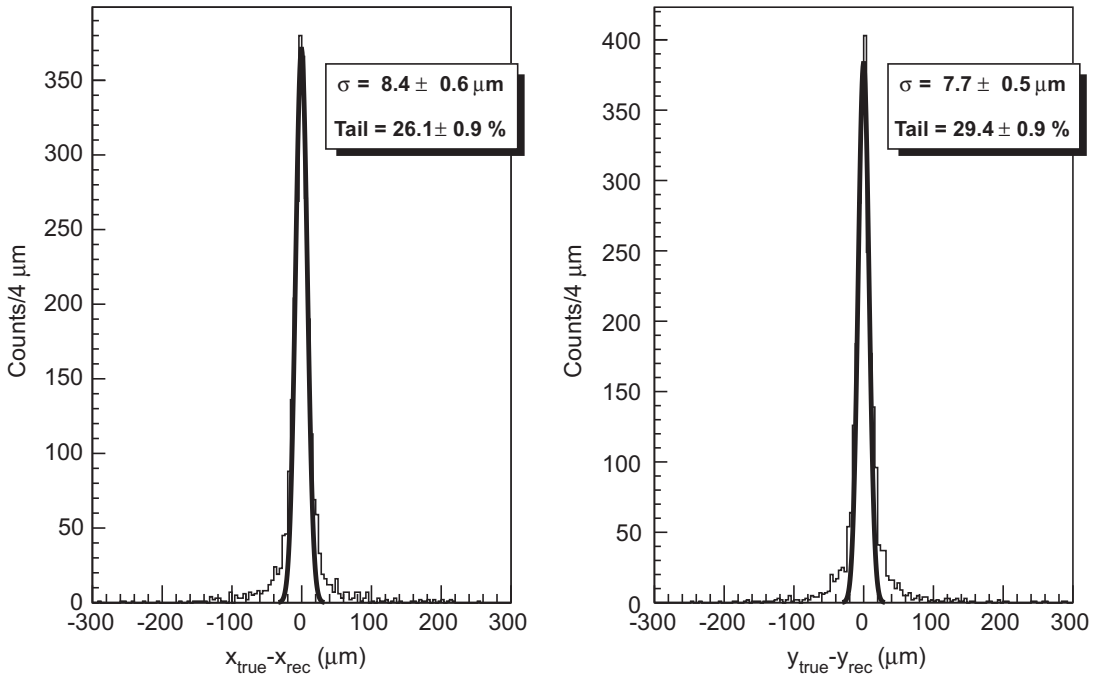


**Fig. 4.** Residual distance between simulated (true) and reconstructed (rec) vertices in *X* (left) and *Y*(right) projections.

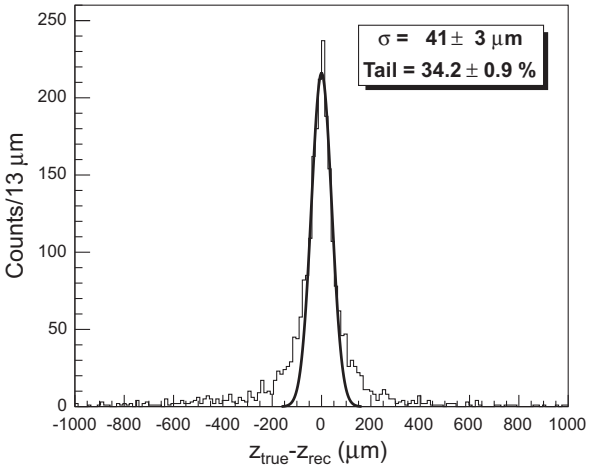


**Fig. 5.** Residual distance between simulated (true) and reconstructed (rec) vertices in the *Z* coordinate.

coordinate (*Z*). Only distributions obtained using vertices reconstructed with the *Probability Distribution Approach* are displayed. Using the *Impact Parameter Approach*, similar results were obtained.

The FIRST experiment global simulation shows that a spatial resolution of the vertex device of 100 μm in *X* and *Y* direction and of 500 μm in *Z* direction is required to attain the desired 9% momentum resolution [17]. The achieved vertex resolutions are of about 11 μm in (*X*,*Y*) plane and less than 60 μm in longitudinal direction (see Figs. 4 and 5). Although the proportion of events outside the Gaussian shape (tails) is quite important (about 30%), only 4% of events is outside the specifications required by FIRST (100 μm in *X* and *Y* direction and of 500 μm in *Z* direction).

Even if the two methods exhibit the same efficiency, the *Probability Distribution Approach* is able to recognise peculiar topologies and performs better in the presence of a pile-up of successive events. The fragmentation of a secondary particle

**Table 4**
Proportion of piled-up events not disentangled by the algorithm. The last column corresponds to the experimental conditions of FIRST.

| 2 piled-up events | 3 piled-up events | 4 piled-up events | FIRST |
|---|---|---|---|
| (4.7 ± 0.2)% | (12.1 ± 0.2)% | (23.0 ± 0.3)% | (2.4 ± 0.1)% |

produced in a primary $^{12}C$ interaction is an example of peculiar topology (concerning about 0.36% of all events). In this case, two different vertices should be reconstructed. The *Probability Distribution Approach* allows us to disentangle the two vertices with an efficiency greater than 99%. Indeed tracks not compatible with a primary vertex point are discarded as explained in Section 2.3.2.

Pile-up happens when two or more separate events occur during the readout time of the CMOS sensors (118 μs per chip). In this study, a single carbon ion impinging the target is considered as one event whether or not fragmentation occurs. In order to estimate the disentangle ability of the *Probability Distribution Approach* procedure, piled-up events were simulated. The case in which two fragmented events pile-up was not included in simulation; the probability that this happen is less than 0.3%. In Table 4, the proportion of piled-up events not disentangled by the algorithm is reported. This proportion increases steadily with the number of piled-up events up to 23% in the case of 4 simultaneous events recorded in the detector.

FIRST experiment allowed us to estimate the total number of pile-up occurrences (about 34%) and the number of events piled-up in each occurrence via the Start Counter detector, a thin scintillator located on the beam path upstream the Beam Monitoring. The Start Counter detector records the arrival time of the beam projectile with a time resolution better than 200 ps and provides the signal to the experiment trigger [17]. The number of events piled-up in each occurrence follows a Poisson distribution with a parameter $\lambda = 0.74$. This distribution represents the measured proportion of piled-up events in FIRST experiment. In the simulation, the number of piled-up events was generated

**Table 5**
Ratio between the number of reconstructed (rec) and simulated (MC) vertices for different vertex multiplicities.

| Multiplicity | $N_{rec}/N_{MC}$ |
|---|---|
| 2 | $0.92 \pm 0.07$ |
| 3 | $1.05 \pm 0.09$ |
| 4 | $0.97 \pm 0.08$ |
| 5 | $1.00 \pm 0.09$ |
| 6 | $1.2 \pm 0.1$ |

accordingly. The total proportion of events which are not disentangled was estimated to $(2.4 \pm 0.1)\%$.

Finally, in the single impinging $^{12}C$ case, the ability of the reconstruction chain to reproduce the vertex multiplicity (*i.e.* number of tracks attached to a given vertex) was evaluated. Each fragmentation event is represented by a vertex that, in the simulation, has a well known multiplicity. However, when a vertex is reconstructed, an under- or an over- estimation of its multiplicity can occur. Indeed, not all tracks are well reconstructed (as defined in Section 3.2), fake tracks can be used to build a vertex and a unique vertex can be splitted into two or more by the vertexing algorithm. Several vertices having different multiplicities were generated and each of them was reconstructed by using the *Probability Distribution Approach* procedure.

The reconstruction impact on multiplicity can be quantified by the ratio between the number of vertices reconstructed with a given multiplicity ($N_{rec}$) and the total number of generated vertices having the same multiplicity ($N_{MC}$). This quantity was computed for multiplicity from 2 to 6. Higher multiplicity was not taken into account, due to their low probability to occur ( $< 5\%$). The results, reported in Table 5, show that this ratio is consistent with one within $2\sigma$ error bars (statistical error) for each multiplicity value. Therefore, the reconstruction chain does not noticeably affect the vertex multiplicity.

## 4. Conclusions

The performances of reconstruction algorithms of the FIRST experiment *Vertex detector* were evaluated on the basis of experimental and simulated data. For each reconstruction step (clustering, tracking and vertexing), more than one algorithm was developed. In each case the most performant was identified and used for the analysis of the FIRST data collection campaign. For the *clustering* step, two algorithms were implemented, both having an high efficiency (more than 99.9%) but one was less time consuming. Tracking procedures based on a combinatorial approach, *TrackingL* and *TrackingH*, reconstruct respectively 10% and 43% more fake tracks than the *TrackingBM* algorithm. The latter is also the fastest among the three methods. Two vertexing methods were implemented, both having a reconstruction efficiency close to 99% and a proportion of fake vertices of 3%. However the probabilistic approach allows us to reconstruct multiple vertices and to disentangle piled-up events. About 34% of FIRST experimental data is affected by pile-up.

The achieved spatial resolution for tracks (better than 10 μm) makes of M26 sensors a promising device for hadrontherapy purpose. In addition, the spatial resolution for vertices (less than 60 μm in longitudinal direction) allows us to reach the required 9% momentum resolution. Thanks to this work, DDCS will be evaluated from the data collected with the FIRST experiment.

## Acknowledgements

We would like to acknowledge Dr. Virgile Bekaert, at Institut Pluridisciplinaire Hubert Curien in Strasbourg, who provided us one of the clustering algorithms presented in this paper.

## References

[1] R.R. Wilson, Radiology 47 (1946) 487.
[2] E. Haettner, H. Iwase, D. Schardt, Radiation Protection Dosimetry 122 (2006) 485.
[3] M. Scholz, Nuclear Instruments and Methods in Physics Research B 161–163 (2000) 76.
[4] M. Kramer, M. Durante, European Physical Journal D 60 (2010) 195.
[5] L. Sihver, Radiation Measurements 44 (2009) 38.
[6] K. Parodi, S. Brons, F. Cerutti, A. Ferrari, A. Mairani, H. Paganetti, F. Sommerer, Proceedings of the Twelfth International Conference on Nuclear Reaction Mechanisms, 2009, p. 509.
[7] T.T. Böhlen, et al., Physics in Medicine and Biology 55 (2010) 5833.
[8] D. Schardt, T. Elsässer, D. Schulz-Ertner, Reviews on Modern Physics 82 (2010) 383.
[9] B. Braunn, et al., Nuclear Instruments and Methods in Physics Research B 269 (2011) 2676.
[10] J. Dudouet, et al., Physical Review C 88 (2013) 024606.
[11] B. Braunn, et al., Journal de physique: Conference Series 420 (2013) 012163.
[12] M. De Napoli, et al., Physics in Medicine and Biology 57 (2012) 7651.
[13] B. Golosio, et al., IEEE Nuclear Science Symposium and Medical Imaging Conference (NSS/MIC), 2012.
[14] E. Spiriti, M. De Napoli, F. Romano, et al., Nuclear Physics B (Proceedings Supplment) 215 (2011) 157.
[15] B. Golosio, et al., IEEE Nuclear Science Symposium and Medical Imaging Conference (NSS/MIC), (2011), p. 2277.
[16] Z. Abou-Haidar, et al., Journal of Instrumentation 7 (2012) 02006.
[17] R. Pleskac, et al., Nuclear Instruments and Methods in Physics Research A 678 (2012) 130.
[18] Ch. Hu-Guo, et al., Nuclear Instruments and Methods in Physics Research 623 (2010) 480.
[19] ⟨http://wiki.gsi.de/cgi-bin/view/FIRST/ReconstructionCode⟩.
[20] ⟨http://root.cern.ch/⟩.
[21] R.O. Duda, P.E. Hart, Communications of the ACM 15 (1972) 1115.
[22] E. Spiriti, private communication.
[23] T.H. Cormen, C.E. Leiserson, R.L. Rivest, C. Stein, Introduction to Algorithms, 2nd ed., MIT Press and McGraw-Hill, 2001, p. 253.
[24] D. Knuth, The Art of Computer Programming 3, 3rd ed., Addison-Wesley, 1997, p. 396.
[25] D.J. Jackson, Nuclear Instruments and Methods in Physics Research A 388 (1997) 247.
[26] ⟨http://geant4.cern.ch⟩.